J. Synchrotron Rad. (1998). **5**, 208–214

High-Energy Inelastic-Scattering Beamline for Electron Momentum Density Study

Y. Sakurai

The Institute of Physical and Chemical Research (RIKEN), SPring-8, Kamigori, Ako-gun, Hyogo 678-12, Japan. E-mail: sakurai@spring8.or.jp

(*Received 4 August 1997; accepted 2 February 1998*)

The advent of synchrotron radiation sources for well polarized and high-energy X-rays offers new opportunities for exploiting Compton scattering spectroscopy as a tool for investigating the electronic and magnetic structures of materials. Recent high-resolution Compton scattering experiments show the unique capability for the study of Fermiology-related issues and electron–electron correlation effects. Intense, high-energy and circularly polarized X-ray sources have improved magnetic Compton scattering spectroscopy from the point of statistical accuracy and momentum resolution. As a next advance, a high-energy inelastic scattering beamline dedicated to Compton scattering spectroscopies is being constructed at SPring-8. The light source is an elliptic multipole wiggler with a periodic length of 12 cm. The beamline includes two experimental stations: one is for high-resolution spectroscopy using 100–150 keV X-rays and the other is for magnetic Compton scattering experiments using circularly polarized 300 keV X-rays. The use of such high-energy X-rays makes it possible to carry out experiments efficiently on samples including heavier elements, such as high-T_c superconductors and 4*f* and 5*f* magnetic materials.

Keywords: high-energy X-rays; elliptic multipole wigglers; Compton scattering spectroscopy; high-T_c superconductors; magnetic materials.

1. Introduction

The Compton profile, $J(p_z)$, is defined as a one-dimensional projection of the ground-state electron momentum density, $n(\mathbf{p})$ (Williams, 1977),

$$J(p_z) = \iint n(\mathbf{p})\,\mathrm{d}p_x \mathrm{d}p_y, \tag{1}$$

where p_x, p_y and p_z are the Cartesian momentum components, the z axis being parallel to the scattering vector. The momentum density, $n(\mathbf{p})$, is given (Lundqvist & Lyden, 1971) as

$$n(\mathbf{p}) = \sum_{\mathbf{k},b,b'} \left[\int \psi_{\mathbf{k},b}(\mathbf{r}) \exp(-i\mathbf{p}.\mathbf{r})\,\mathrm{d}\mathbf{r}\right]^* \times \left[\int \psi_{\mathbf{k},b'}(\mathbf{r}) \exp(i\mathbf{p}.\mathbf{r})\,\mathrm{d}\mathbf{r}\right] N_{b,b'}(\mathbf{k}), \tag{2}$$

where $\psi_{\mathbf{k},b}(\mathbf{r})$ is the wavefunction and $N_{b,b'}(\mathbf{k})$ is the occupation number of the quasiparticle states with wavevector $\mathbf{k}$ in the band b and b'. Therefore, the Compton profile, $J(p_z)$, contains fingerprints of Fermi surface breaks in the underlying three-dimensional momentum distribution, $n(\mathbf{p})$. The size of the Fermi surface discontinuity in the momentum density and its possible renormalization due to electron–electron correlation is a fundamental property of the ground-state electronic structure, inaccessible to other $\mathbf{k}$-resolved spectroscopies such as angle-resolved photoemission, the de Haas–van Alphen effect and positron annihilation. If the incident X-rays have a degree of circular polarization, one can measure the magnetic Compton profile on ferromagnetic materials, which provides information about spin-dependent ground-state electron momentum density.

Compton scattering experiments with γ-ray sources and X-ray tubes have been extensively performed on various kinds of materials (Cooper, 1985). However, these photon sources are not optimal for high-resolution and magnetic Compton scattering experiments. Recent advents of high-intensity, high-energy and well polarized synchrotron radiation sources offer new opportunities for developing Compton scattering as a tool for investigating Fermiology-related issues, electron–electron correlation effects and ferromagnetism in a wide class of materials (Manninen *et al.*, 1996; Sakurai *et al.*, 1992; Sakai, 1996).

Synchrotron radiation-based high-resolution Compton scattering experiments carried out so far have been limited to low- and medium-Z elements, namely up to 3*d* elements (Sakurai *et al.*, 1994, 1998; Blass *et al.*, 1995) since the cross section of the photoelectric effect becomes larger than that of Compton scattering on heavier elements at previously available X-ray energies of ~60 keV. Concerning magnetic Compton spectroscopy, experiments using a pure-Ge solid-state detector (SSD) were extensively performed for 3*d* and 4*f* metals and alloys using circularly polarized 45–60 keV X-rays from an elliptic multipole wiggler (Sakai, 1996). In the case of 4*f* elements, however, the counting

rates were dominated by fluorescent X-rays. Recent magnetic Compton scattering experiments with much higher energy X-rays (84.4, 167.2, 256.0 keV) show that the use of such higher energy X-rays improves the overall momentum resolution of the experiments which use a pure-Ge SSD (McCarthy *et al.*, 1997). Then, in order to measure efficiently the Compton profile of high-Z elements, such as high-T_c superconductors and 4*f* and 5*f* ferromagnets, X-rays of energy higher than 100 keV are indispensable for both high-resolution and magnetic Compton scattering experiments.

With this motivation, a beamline for high-energy inelastic-scattering (Compton scattering) experiments is under construction at SPring-8. The beamline (BL08W) has two experimental stations: one is for high-resolution spectroscopy with a momentum resolution of better than 0.1 atomic units (a.u.) using 100–150 keV X-rays, and the other is for magnetic Compton spectroscopy with a resolution of 0.5 a.u. using circularly polarized 300 keV X-rays.

In §2, details of the high-energy inelastic scattering beamline are described. In §3, recent progress in high-resolution Compton scattering spectroscopy is presented in order to demonstrate its potential. Recent magnetic Compton scattering experiments are not presented in this paper; instead the reader is referred to Sakai (1996) for details of recent magnetic Compton scattering experiments using a multi-element solid-state detector.

2. Description of high-energy inelastic-scattering beamline (BL08W)

2.1. *Target materials at the beamline*

There are several advantages of using much higher energy X-rays. One is to increase the amount of Compton scattered X-rays and magnetic effects, while reducing the background noise due to fluorescent X-rays (McCarthy *et al.*, 1997). They also guarantee the validity of the impulse approximation for high-Z elements. Another advantage is that they increase the mean free path of the recoil electrons, which produces a better counting rate in coincident Compton scattering experiments (Bell *et al.*, 1991; Kurp *et al.*, 1996; Itou *et al.*, 1998).

Fig. 1 shows a plot of recent high-resolution Compton scattering experiments and the research targets at the high-energy inelastic scattering beamline (BL08W). The use of 100–150 keV X-rays will enable us to extend research of Fermiology-related issues and the electron–electron correlation effects for high-T_c superconductors, heavy-electron systems, 4*d* and 4*f* metals and alloys.

Fig. 2 shows a similar plot for magnetic Compton scattering experiments with a moderate resolution using a pure-Ge solid-state detector. Experiments using high-energy X-rays will improve efficiencies in measurements of Compton profiles by reducing the amount of fluorescent X-rays. We will be able to carry out a systematic research program, including temperature-variation experiments. Another advantage of 300 keV X-rays is enhancement of the magnetic effects.

2.2. *Insertion device and front end*

The beamline design is based on the use of an elliptic multipole wiggler (EMPW) with a critical energy of 42.6 keV at the minimum gap of 20 mm (Kitamura, 1998). The periodic length of the magnetic array is 12 cm and the total length of the insertion device is 4.5 m. The maximum total radiation power is 18.7 kW at a beam current of 100 mA. The calculated total flux spectrum emitted from the EMPW is shown in Fig. 3. Graphite and aluminium filters are placed in the beamline front end to absorb the low-energy part of the synchrotron radiation. After the filters, the heat load on the monochromators is reduced to several hundred watts without serious loss of the high-energy X-ray flux, as shown in Fig. 3.

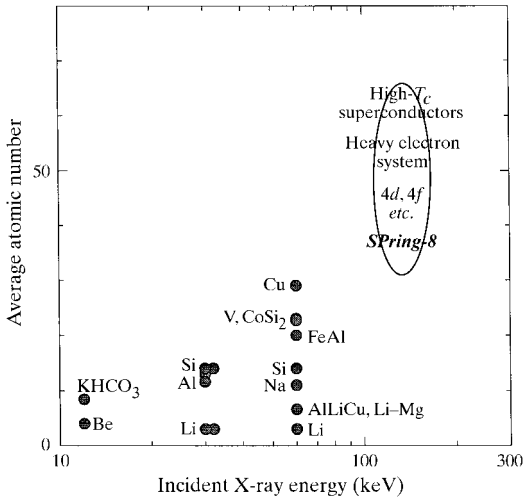

Figure 1
Recent high-resolution Compton scattering experiments and targets at SPring-8.

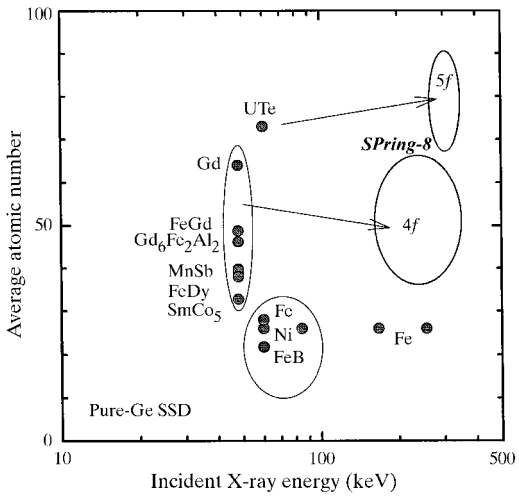

Figure 2
Recent magnetic Compton scattering experiments and targets at SPring-8.

2.3. *Optics and experimental stations*

Fig. 4 shows the schematic layout of the beamline in the experimental hall. The beamline has two experimental stations: station A is for magnetic Compton spectroscopy with a resolution of 0.5 a.u. using circularly polarized 300 keV X-rays, and station B is for high-resolution spectroscopy with a momentum resolution of better than 0.1 a.u. using 100–150 keV X-rays. Two monochromators (Yamaoka *et al.*, 1998) are installed in the optics hutch: one is an asymmetric Johan monochromator which produces a line focus with a size of 3 mm × 0.5 mm for magnetic Compton spectroscopy. The diffraction plane is Si 771 with an asymmetric angle of 1°. The other is a doubly bent monochomator for high-resolution spectroscopy. The diffraction plane is Si 400. The curvatures are designed to achieve the best focus (1.5 mm × 1.8 mm) at an X-ray energy of 115 keV (uranium *K*-edge) since the absorption edge is used for the adjustment of the monochromator.

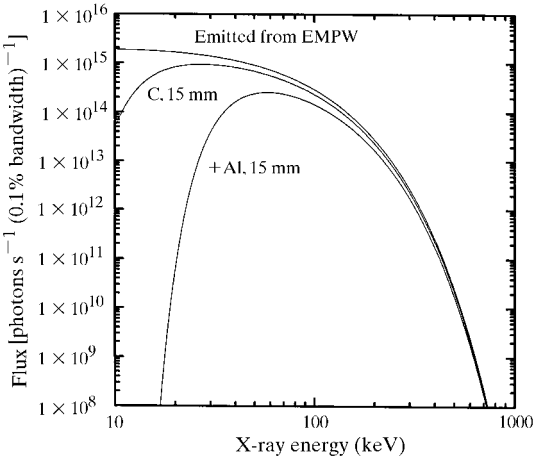

Figure 3
Calculated total flux of the EMPW and that after the filters.

Experimental station A houses a magnetic Compton spectrometer with a combination of a ten-element Ge solid-state detector and a superconducting magnet. The momentum resolution is expected to be 0.5 a.u. for an incident X-ray energy of 300 keV, when the detector is placed at 1 m from the sample and the counting rate of each is less than $\sim 5 \times 10^4$ counts s^{-1}. The maximum magnetic field of the magnet is 3 T and is reversed within 5 s. The superconducting magnet is strong enough to magnetize hard magnetic materials such as 4*f* rare-earth elements and alloys. Vaporized He is recondensed by a refrigerator to realize a maintenance-free operation of the magnet over a week. Samples can be cooled to 10 K by another refrigerator. The photon flux and on-axis circular polarization at the sample position are expected to be $\sim 10^{11}$ photons s^{-1} and $\sim$0.7, respectively, at 300 keV.

Experimental station B will accommodate a high-resolution spectrometer with a designed momentum resolution of better than 0.1 a.u. The spectrometer consists of a Cauchois-type Si 440 analyser and a position-sensitive detector (Sakai *et al.*, 1995) with a spatial

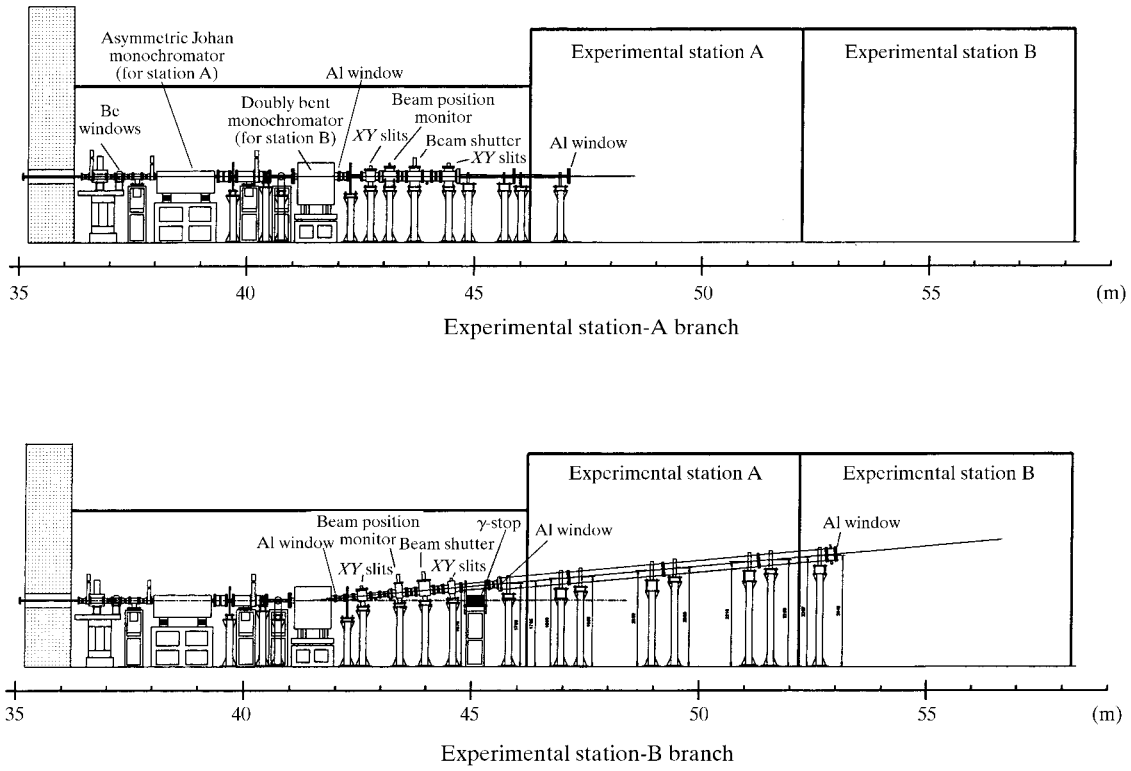

Figure 4
Schematic layout of the beamline (BL08W).

resolution of 0.2 mm. The photon flux is expected to be $\sim 10^{13}$ photons s^{-1} at 115 keV.

3. Recent high-resolution spectroscopy

3.1. *Beryllium*

It is known that the Fermi surface of Be consists of two kinds of surfaces: the hole-like 'coronet' and the electron-like 'cigar'. Fig. 5 shows the first two Brillouin zones as well as the coronets and cigars. Beryllium contains four electrons per unit cell, which can be, in principle, accommodated in two full bands. Actually, the third band is partially occupied and yields the cigars, and an equal number of remaining holes then form the coronet. The experimental Compton profiles are shown in Fig. 6, together with those of the all-electron-charge self-consistent KKR (Korringa–Kohn–Rostoker) band theoretical calculations based on the local density approximation (LDA) (Itou *et al.*, 1997; Hamalainen *et al.*, 1996). The theoretical profiles have been convoluted with a Gaussian of 0.08 a.u. FWHM to reflect the experimental resolution. Fig. 6 shows reasonable agreements between experiment and theory concerning the overall shapes. However, the experimental profiles give lower momentum density than the theoretical ones at low momenta, and higher momentum density at high momenta. This feature is in accord with the earlier γ-ray Compton work (Hansen *et al.*, 1979) and high-resolution experiments (Loupias & Petiau, 1980) on Be. This is common in studies of other materials (Shiotani *et al.*, 1993; Sakurai *et al.*, 1995; Bellin *et al.*, 1995; Schuelke *et al.*, 1996). Contrary to these results, ultra-high-resolution experiments on Be with a momentum resolution of 0.02 a.u. (Hamalainen *et al.*, 1996) show higher momentum density than the theoretical ones at low momenta. The significantly different features in the height of the Compton profile are probably due to the different methods of the normalization of the profile. Fig. 7 shows the first derivatives of the Compton profiles. Concerning the Fermi surface signatures, a close analysis of the theoretical results shows that the feature A in the [1120] direction is due to the cigars, the broad feature B arises from a combination of the coronet and cigars, and the sharp dip C is from the surface of the cigars in the third Brillouin zone around the K-point in the basal plane. In the [0001] direction, the feature D arises from the coronet, the feature E from the cigars, and the big dip F is due to the Brillouin zone boundary. The broadened Fermi surface features are observed in the experimental first-derivative curves compared with the theoretical ones, particularly around the features B and C.

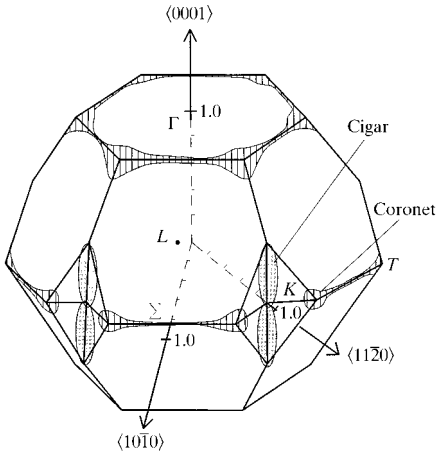

Figure 5
Fermi surface and first two Brillouin zones of Be.

The facts that the experimental Compton profiles are lower at low momenta and the first-derivative curves show broadened Fermi surface features are due to electron–electron correlation effects, mostly due to the non-unity and non-zero nature of the occupation function, $N_{b,b'}(\mathbf{k})$ in (2), which is not taken into account in the LDA-based band theory (Bauer & Schneider, 1983).

3.2. *Lithium*

Similar discrepancy has been observed between recent experimental Compton profiles (Sakurai *et al.*, 1995; Schuelke *et al.*, 1996) and LDA-based band theoretical computations for Li. Both experimental valence Compton profiles show excellent agreement. Recently, Kubo performed a first-principle computation of the momentum density of Li using the spectral density based on the GW approximation (Kubo, 1996, 1997). Fig. 8 shows the experimental Compton profiles of Li along the [111] direction, together with that computed by the LDA-based FLAPW (full-potential linearized augmented-plane wave) scheme and that computed with GW approximation. Employment of the GW approximation lowers the profiles at low momenta. This demonstrates the importance of including the electron–electron correlation effects for a satisfactory description of the observed momentum density.

3.3. *High-resolution magnetic Compton scattering spectroscopy on Fe–5.8at.%Si*

The momentum distribution of electrons involved in ferromagnetism is of particular importance. In terms of band theory it provides information about spin-dependent occupation in momentum space and spin-dependent wavefunctions in the ground state. The Compton profiles, $J(p_z)$, in (1) are related to the measured double-differential cross section by

$$\mathrm{d}^2\sigma/\mathrm{d}\Omega\mathrm{d}\omega_2 = r_0^2\mathbf{A}^2(\omega_2/\omega_1)J(p_z), \tag{3}$$

where ω_1 and ω_2 are the incident and scattered photon energies, respectively, r_0 is the classical electron radius and $\mathbf{A}$ is proportional to the scattering amplitude, which is written as

$$\mathbf{A} = a + \mathbf{b}.\mathbf{S}, \tag{4}$$

where the first term is for charge scattering and the

second term corresponds to magnetic scattering from the electron spin, **S** (Platzman & Tzoar, 1970). The vector **b** is determined by the photon energy and the scattering angle. If the incident photon has a significant degree of circular polarization, there is an interference term which carries information on the spin-dependent electron momentum density. It is convenient to rewrite (3) in terms of the total Compton profile, $J(p_z)$, and magnetic Compton profile, $J_{\rm mag}(p_z)$,

$$\mathrm{d}^2\sigma/\mathrm{d}\Omega\mathrm{d}\omega_2 = C_{\rm charge}(\omega_2/\omega_1)J(p_z) + C_{\rm mag}(\omega_2/\omega_1)J_{\rm mag}(p_z), \quad (5)$$

Here,

$$J(p_z) = J_{\rm maj}(p_z) + J_{\rm min}(p_z) \quad (6)$$

and

$$J_{\rm mag}(p_z) = J_{\rm maj}(p_z) - J_{\rm min}(p_z), \quad (7)$$

where

$$J_{\rm maj}(p_z) = \iint n_{\rm up}(\mathbf{p})\,\mathrm{d}p_x\mathrm{d}p_y \quad (8)$$

and

$$J_{\rm min}(p_z) = \iint n_{\rm down}(\mathbf{p})\,\mathrm{d}p_x\mathrm{d}p_y. \quad (9)$$

$n_{\rm up}(\mathbf{p})$ and $n_{\rm down}(\mathbf{p})$ are the electron momentum densities of majority-spin and minority-spin electrons, respectively. $C_{\rm charge}$ and $C_{\rm mag}$ are coefficients depending on the experimental conditions. The magnetic Compton profile is then obtained experimentally by subtracting data sets taken with the magnetization field direction reversed. The total profile is obtained by adding the data sets. With an experimentally determined magnetic Compton profile, $J_{\rm mag}(p_z)$, and a total profile, $J(p_z)$, it is possible to separate the Compton profiles of the majority-spin and minority-spin electrons, $J_{\rm maj}(p_z)$ and $J_{\rm min}(p_z)$.

Fig. 9 shows the experimental total valence electron, majority-spin and minority-spin electron Compton profiles of Fe–5.8at.%Si, together with those of FLAPW computations for pure Fe (Sakurai *et al.*, 1994). The experimental momentum resolution is 0.13 a.u. It demonstrates that with a high-resolution spectrometer and an elliptic multipole wiggler it is actually possible to measure a total profile and a magnetic profile, and

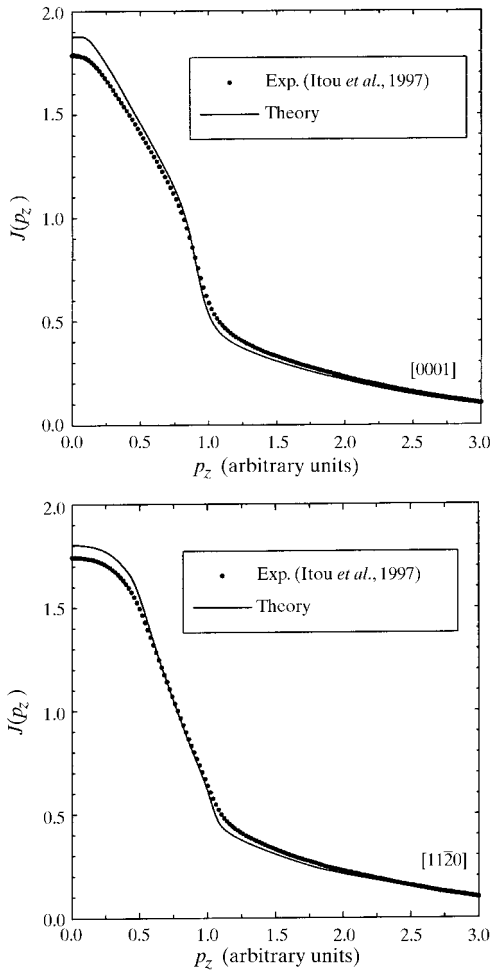

Figure 6
Experimental and theoretical Compton profiles of Be.

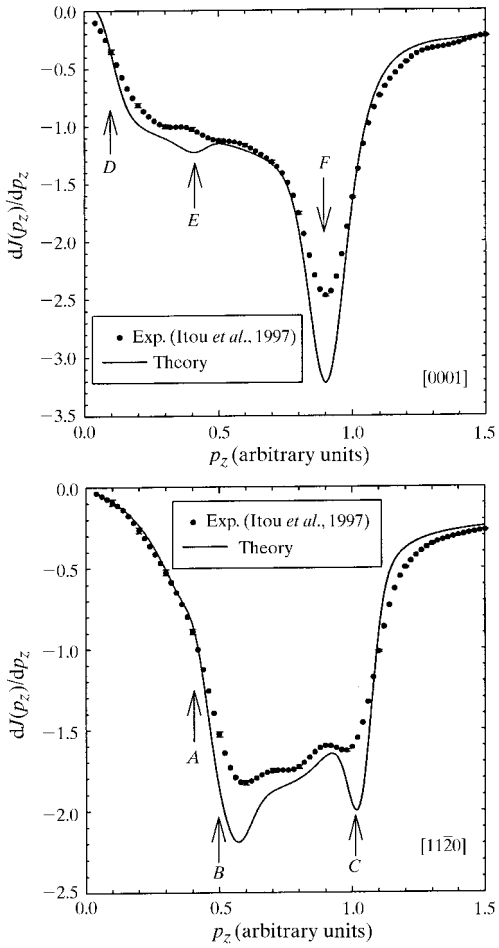

Figure 7
First-derivative curves of experimental and theoretical Compton profiles of Be.

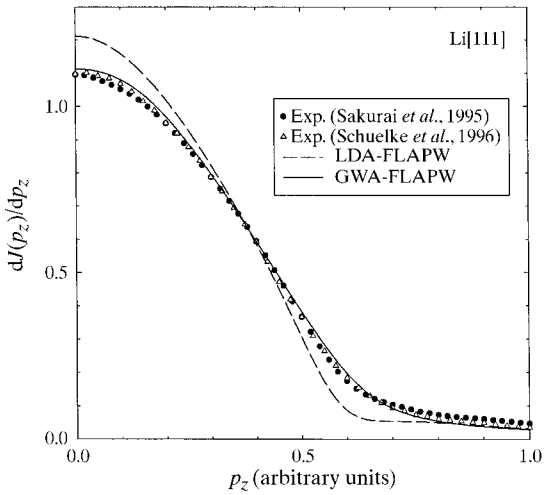

Figure 8
Experimental Compton profile of Li along the [111] direction, together with those of the LDA-based FLAPW and the GW approximation calculations

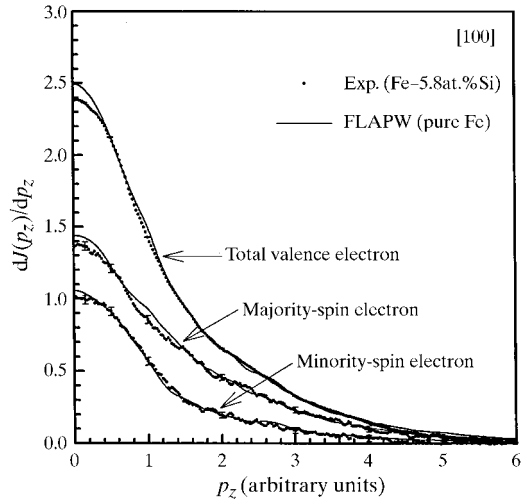

Figure 9
Experimental total valence electron, majority-spin and minority-spin electron Compton profiles of Fe–5.8at.%Si, together with those of FLAPW calculations for pure Fe.

thus the majority-spin and minority-spin electron momentum distributions with a momentum resolution of 0.1 a.u.

4. Summary

The potential of Compton scattering spectroscopies has been established as a tool for investigating Fermiology-related issues, electron–electron correlation effects and magnetic structures in materials. The use of higher energy X-rays removes the limitation in atomic number of materials. The applicability of the Compton techniques in wide classes of simple and complex systems can thus be anticipated in the high-energy inelastic scattering beamline (BL08W) at SPring-8.

It is a pleasure to acknowledge many important conversations with Professor Shiotani and Professor Sakai. The author wishes to thank Professor Kitamura for helpful discussions on the insertion device, and Dr Kawata for suggestions and discussions on the monochromators. Thanks are also given to Dr Yamaoka for valuable discussions on the monochromators and Dr Mizumaki for his collaboration. The author also thanks Professor Bansil and Professor Kubo for discussing the experimental results.

References

Bauer, G. E. W. & Schneider, J. R. (1983). *Solid State Commun.* **47**, 673–679.
Bell, F., Tschentscher, Th., Schneider, J. R. & Rollason A. J. (1991). *J. Phys. Condens. Matter*, **3**, 5587–5601.
Bellin, Ch., Loupias, G., Manuel, A. A., Jarlborg, T., Sakurai, Y., Tanaka, Y. & Shiotani, N. (1995). *Solid State Commun.* **96**, 563–567.
Blass, Y., Redinger, J., Manninen, S., Honkimaki, V., Hamalainen, K. & Suortti, P. (1995). *Phys. Rev. Lett.* **74**, 1984–1987.
Cooper, M. J. (1985). *Rep. Prog. Phys.* **48**, 415–481.
Hamalainen, K., Manninen, S., Kao, C. C., Caliebe, W., Hastings, J. B., Bansil, A., Kaprzyk, S. & Platzman, P. M. (1996). *Phys. Rev. B*, **54**, 5453–5459.
Hansen, N. K., Pattison, P. & Schneider, J. R. (1979). *Z. Phys. B*, **35**, 215–229.
Itou, M., Kishimoto, S., Kawata, H., Ozaki, M., Sakurai, H. & Itoh, F. (1998). *J. Synchrotron Rad.* **5**, 676–678.
Itou, M., Sakurai, Y., Ohata, T., Bansil, A., Kaprzyk, S., Tanaka, Y., Kawata, H. & Shiotani, N. (1997). *J. Phys. Chem. Solids.* To be published.
Kitamura, H. (1998). *J. Synchrotron Rad.* **5**, 184–188.
Kubo, Y. (1996). *J. Phys. Soc. Jpn*, **65**, 16–18.
Kubo, Y. (1997). *J. Phys. Soc. Jpn*, **66**, 2236–2239.
Kurp, F. F., Tschentscher, Th., Schulte-Schrepping, H., Schneider, J. R. & Bell, F. (1996). *Europhys. Lett.* **53**, 61–70.
Loupias, G. & Petiau, J. (1980). *J. Phys. Paris*, **41**, 265–274.
Lundqvist, B. I. & Lyden, C. (1971). *Phys. Rev. B*, **4**, 3360–3370.
McCarthy, J. E., Cooper, M. J., Lawson, P. K., Timms, D. N., Manninen, S., Hamalainen, K. & Suortti, P. (1997). *J. Synchrotron Rad.* **4**, 102–109.
Manninen, S., Honkimaki, V., Hamalainen, K., Laukkanen, J., Blaas, C., Redinger, J., McCarthy, J. E. & Suortti, P. (1996). *Phys. Rev.* **53**, 7714–7726.
Platzman, P. M. & Tzoar, N. (1970). *Phys. Rev. B*, **2**, 3556–3559.
Sakai, N. (1996). *J. Appl. Cryst.* **29**, 81–99.
Sakai, N., Koizumi, A., Sato, T., Sato, K. & Ueki, T. (1995). Private communication.
Sakurai, Y., Ito, M., Urai, T., Tanaka, Y., Sakai, N., Iwazumi, T., Kawata, H., Ando, M. & Shiotani, N. (1992). *Rev. Sci. Instrum.* **63**, 1190–1193.

Sakurai, Y., Kaprzyk, S., Bansil, A., Tanaka, Y., Stutz, G., Kawata, H. & Shiotani, N. (1998). In preparation.

Sakurai, Y., Tanaka, Y., Bansil, A., Kaprzyk, S., Stewart, A. T., Nagashima, Y., Hyodo, T., Nanao, S., Kawata, H. & Shiotani, N. (1995). *Phys. Rev. Lett.* **74**, 2252–2255.

Sakurai, Y., Tanaka, Y., Ohata, T., Watanabe, Y., Nanao, S., Ushigami, Y., Iwazumi, T., Kawata, H. & Shiotani, N. (1994). *J. Phys. Condens. Matter*, **6**, 9469–9475.

Schuelke, W., Stutz, G., Wohlert, F. & Kaprolat, A. (1996). *Phys. Rev. B*, **54**, 14381–14390.

Shiotani, N., Tanaka, Y., Sakurai, Y., Sakai, N., Ito, M., Itoh, F., Iwazumi, T. & Kawata, H. (1993). *J. Phys. Soc. Jpn*, **62**, 239–245.

Williams, B. G. (1977). *Compton Scattering.* New York: McGraw-Hill.

Yamaoka, H., Mochizuki, T., Sakurai, Y. & Kawata, H. (1998). *J. Synchrotron Rad.* **5**, 699–701.